

COMPARISONS OF OBSERVATIONS AND SIMULATIONS OF THE MARS POLAR ATMOSPHERE

D. J. McCleese¹, A. Kleinboehl¹, D. M. Kass¹, J. T. Schofield¹, R. J. Wilson² and S. Greybush³. ¹Jet Propulsion Laboratory, California Institute of Technology, Pasadena, CA; ²NOAA Geophysical Fluid Dynamics Laboratory, Princeton, NJ; and ³Penn State, University Park, PA. (Daniel.J.McCleese@jpl.nasa.gov)

Introduction: Recent advances in algorithms used to process data from the Mars Climate Sounder (MCS) [1] permit the study of the Mars polar atmosphere with unprecedented spatial and temporal resolution and coverage. We have used this improved observational record in comparisons with General Circulation Models (GCM) and reanalysis. To date, limitations in the observations have made more difficult studies of the strengths and weaknesses in simulations of the Martian polar atmosphere, such as the polar vortices. No less important are recent advances in reanalysis applied to MCS data, which has the potential for improving understanding by producing high-fidelity simulations of atmospheric fields not directly observed or retrieved and at spatial and temporal resolutions not available to existing measurement techniques.

MCS Observations: Limb and near-nadir observations by the Mars Climate Sounder onboard the Mars Reconnaissance Orbiter (MRO) provide vertical profiles of temperature and the opacities of dust and water ice [2]. Profiles of the opacity of CO₂ ice in the winter polar atmosphere are inferred from spectral and thermal information (see below). The vertical coverage of MCS observations extends from near the surface to 80 km altitude with a vertical resolution 5 km. MRO is in a 3 am–3 pm near-polar orbit, which is well suited to studies of seasonal and interannual variability of the atmosphere.

MCS measures atmospheric radiance in 5 spectral channels in the mid-infrared and in the 3 far-infrared, plus a visible to near-infrared channel. Each spectral channel comprises a 21-element detector array. Together they provide simultaneous measurements and vertical profiles in all 9-channels when directed via a scan mirror toward the limb [3].

Recent advances in the MCS data processing algorithm have significantly improved the retrieval of atmospheric properties, e.g. temperature and aerosol opacities, when strong horizontal gradients exist along the limb optical path [4]. This 2D radiative transfer scheme enables the investigation of the winter polar atmosphere, where strong latitudinal gradients are present, particularly in the polar vortex, and a more meaningful comparison of retrieved quantities from

MCS measurements with simulations. Previous versions of MCS data products for these extreme conditions may have had systematic biases.

The operational MCS retrieval algorithm used to process these data does not yet distinguish between dust in the atmosphere and CO₂ ice aerosol. Our data products identify CO₂ ice as dust (see figure 1 below). Several characteristics of aerosol opacity in the MCS data in the winter polar regions, principally spectral properties [5], temperature dependence and location, strongly suggest that the source of retrieved is, in fact, CO₂ ice. The appearance of ice is consistent with the atmosphere being at (and at times below) the condensation temperature of CO₂ [6]. In this paper we use the frost point to identify CO₂ ice aerosol.

Mars General Circulation Models: Observations of temperature and aerosols of dust, H₂O ice, and inferred CO₂ ice are compared with results from the LMD Mars Climate Database (MCD) [7], and Ensemble Mars Reanalysis System (EMARS) [8], which assimilates MCS temperature measurements. Comparisons between simulations are also made, emphasizing the impact of data in the region of the polar vortices.

Results: In Figure 1, we show a zonally averaged vertical cross-section of Martian atmospheric temperature, together with mass mixing ratios (ppm) of aerosols in southern winter at L_s=107°. Observations of the nightside (~3:30 am) are shown on the leftside of each panel, and dayside (~3:30 pm) on the right. Because Figure 1 shows the southern polar night, day-night temperatures (top panel) are nearly symmetric near the pole.

The southern polar vortex can be seen to be well established, with minimum temperatures between 120–130 K centered at ~20 Pa (~30 km altitude), and estimating from temperature alone the vortex extends from 55°S to the pole. Atmospheric dust extends from the equator to ~35°S, where an abrupt reduction in dust opacity occurs. Substantial opacity due to aerosols exists in the core of the vortex, a part of which is interpreted to be CO₂ ice (center panel). H₂O ice is also present in the vortex core (lower panel). Analysis of individual vertical profiles of H₂O aerosol from MCS

strongly suggest that water is entering the southern vortex from above, possibly transported by the Hadley cell circulation.

Inspection of MCS data in time-steps of 5° of L_s , for $L_s=10^\circ$ through 110° in the south, shows that aerosols are an excellent indicator of the state and evolution of the north and south polar atmosphere and their respective vortices (shown in the paper). Among the features evident as the time series approaches mid-winter is the confinement of dust to latitudes equatorward of 50° . In the core of the vortex, as defined by the boundaries of the temperature minimum, CO_2 ice clouds or hazes develop, and H_2O ice aerosol form.

The onset, evolution and ultimate morphology of the northern and southern winter polar atmosphere exhibit differences in many important respects. The observations show that while the southern vortex is remarkably stable dynamically, in the north the vortex is frequently perturbed, likely a dynamical impact of dust in the atmosphere in the south through the Hadley circulation. The northern vortex is also more vertically confined to the middle atmosphere, and water ice aerosol is more abundant. Again, contrasts between the north and south vortices, and comparisons with GCM results and reanalysis will be presented and discussed.

Figure 2 is an example of output from the LMD MCD simulations for southern winter ($L_s=90^\circ-120^\circ$). In this figure, we show the equator to pole cross-section of temperature, as well as mass mixing ratios of dust and H_2O ice, comparable with observations in Figure 1. The thermal structure of the vortex in the MCD (top panel) is in good agreement with the observations. Dust is observed to lie in a broad layer centered on 100 Pa, whereas the simulation (center panel) shows dust throughout the lower atmosphere and extending to higher latitudes. MCD includes a CO_2 cycle with condensation occurring on the surface when the temperature falls to the frost point, but it does not track CO_2 ice as an aerosol. Thus, comparison of the simulation with observations in the core of the vortex can be made for dust only. Dust amounts are low in the vortex core in both. The subtropical H_2O ice clouds in the simulation (bottom panel) occur lower in the atmosphere and at higher concentrations than is seen in the observations. The lower limit of the vertical range of MCS observations, approximately 5-10 km, rules out study of the low altitude aerosols spanning the polar region in the MCD.

Figure 3 presents results of EMARS, which is a reanalysis using the MCS temperature observations (Figure 1, top panel). Zonally averaged vertical cross-sections of temperature and mixing ratios of dust and H_2O ice for $L_s 98.4^\circ$ are shown in the center and bot-

tom panels. This relatively early version of EMARS does not assimilate vertical profiles of dust. And, like MCD, EMARS simulation of the CO_2 cycle does not include CO_2 cloud microphysics. Comparisons between the results of EMARS and the observations in all three fields do not differ greatly from those of the MCD.

Acknowledgments: Part of this work was presented at the Mars Polar Conference (2016). This work was performed at the Jet Propulsion Laboratory, California Institute of Technology, under contract with the National Aeronautics and Space Administration. © 2016, California Institute of Technology. Government sponsorship acknowledged.

References: [1] Kleinboehl, A. et al. (2016) JQSRT, submitted. [2] McCleese, D. J. et al. (2010) JGR, 115, E12016. [3] McCleese, D. J. (2007) JGR, 112, E002790. [5] Hayne, P. et al. (2012) JGR, 117, E004040. [6] Kleinboehl, A. et al. (2016) Mars Polar Conference 6. [7] Forget, F., et al. (1999), JGR, 104, E10. [8] Greybush, S. J. et al. (2012) JGR, 117, E11008.

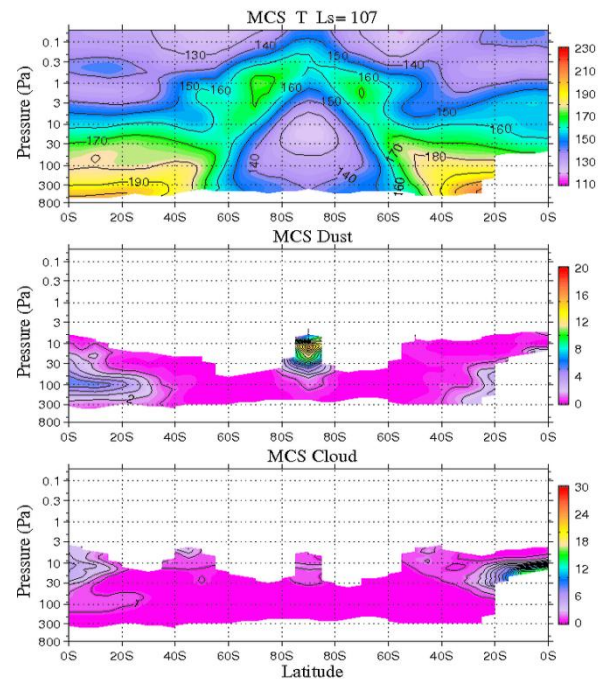


Figure 1: Temperature structure (top), and dust and water ice mass mixing ratios in ppm (bottom) of the southern hemisphere as seen by the Mars Climate Sounder in winter ($L_s=85^\circ-90^\circ$) of Mars Year 29. Profiles retrieved with a two-dimensional retrieval algo-

erithm were zonally averaged in 5° of latitude. The middle panel is labeled “MCS Dust” but the aerosol mapped by MCS is understood to be CO_2 ice in the vicinity of the temperature minimum between approximately 60° S and the pole.

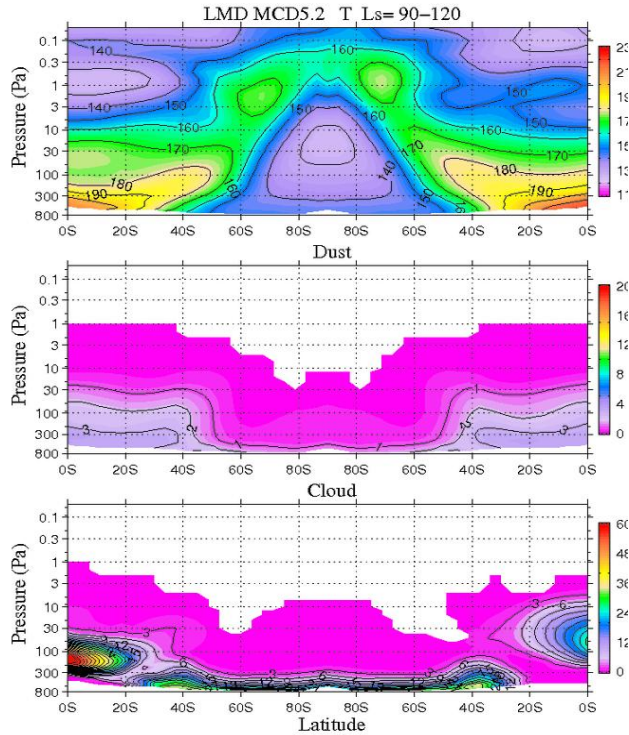


Figure 2: LMD MCD simulations of zonal cross-sections of temperature structure (top), and the mass mixing ratios (ppm) of dust (center) and water ice (bottom) for the southern hemisphere in southern winter ($L_s=90^\circ-120^\circ$).

Turning to the northern hemisphere, Figure 4 shows a MCS zonally averaged vertical cross-section of atmospheric temperature, together with mass mixing ratios (ppm) of aerosols in northern winter at $L_s=287^\circ$. In the north, temperatures are generally warmer in the lower atmosphere compared with the south in the same season, with the exception of the polar vortex where temperatures are similar. The atmosphere between 0.3-3 Pa poleward of 75° N over the vortex is up to 20K warmer than in the south. A detached layer of dust is present at 30 Pa equatorward of 15° N, both day and night, that is not seen in southern winter.

CO_2 ice is present in the core of the vortex, but at a lower amount than is seen in the south (middle panel). Clouds of water ice are present in the middle atmosphere, which do not appear in the southern winter (bottom panel).

LMD simulations for $L_s=270^\circ-300^\circ$ are shown in Figure 5. Poleward of 40° N, temperatures above 10 Pa are warmer than those observed. MCS temperatures

near 3 Pa and $35^\circ-55^\circ$ N are significantly colder than in the simulation and EMARS reanalysis (Figure 6).

Both LMD and EMARS show low altitude water clouds extending from mid to high latitudes, not found in the observations. The reanalysis in Figure 6 gives larger H_2O cloud amounts at mid-altitudes, but neither scheme captures clouds observed poleward of 30° N.

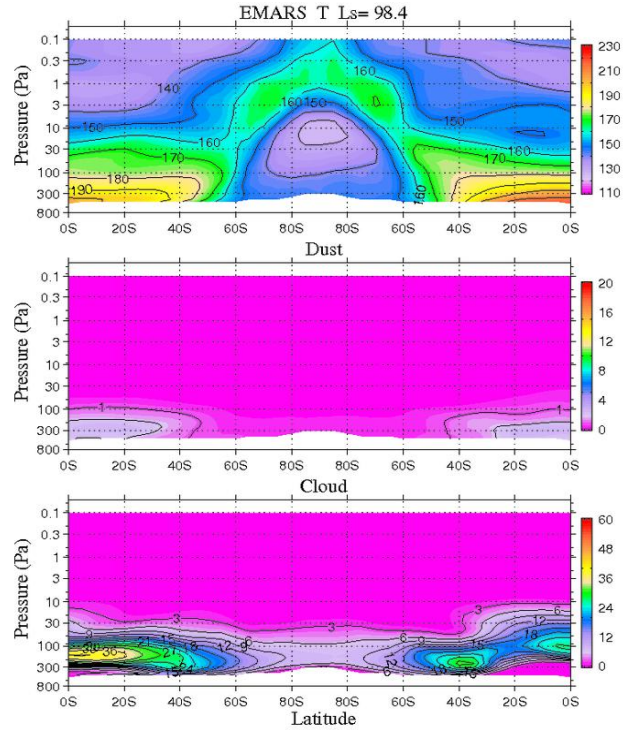


Figure 3: EMARS zonal cross-sections of temperature structure (top), and mass mixing ratios of dust (center) and water ice (bottom) in southern winter ($L_s=98.4^\circ$) obtained from reanalysis of MCS data (Figure 1).

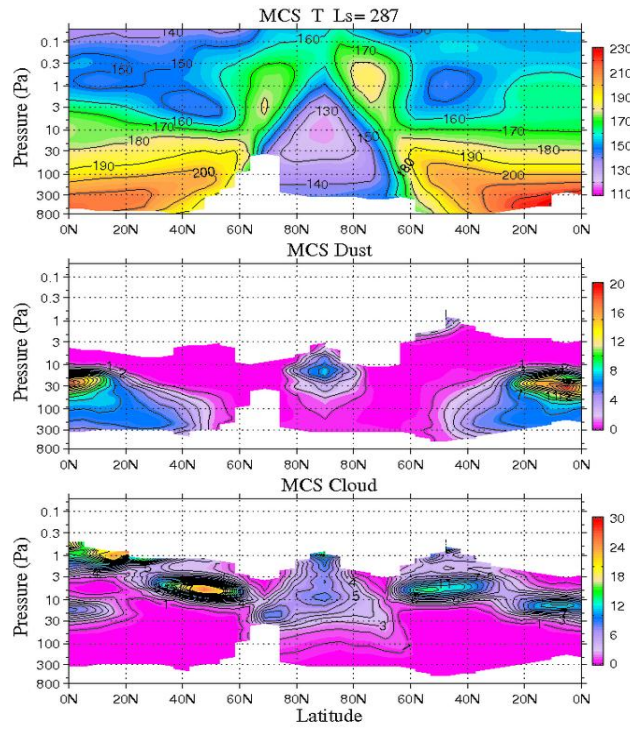


Figure 4: MCS observations of northern winter ($L_s=287^\circ$) in MY 29. (Figure 4 is equivalent to Figure 1 for northern hemisphere, with CO_2 ice over N. pole).

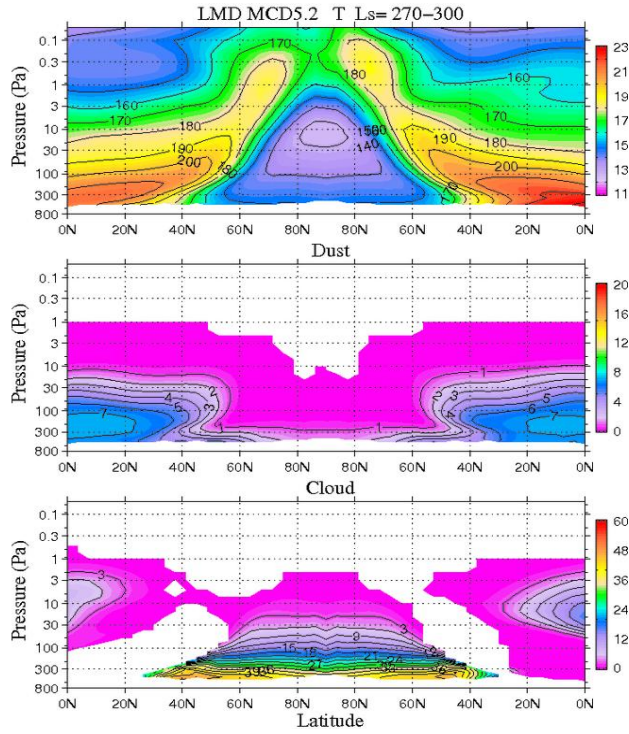


Figure 5: LMD MCD northern hemisphere simulations of zonal cross-sections of temperature structure (top), and the mass mixing ratios (ppm) of dust (center) and water ice (bottom) for northern winter ($L_s=270^{\circ}$ - 300°).

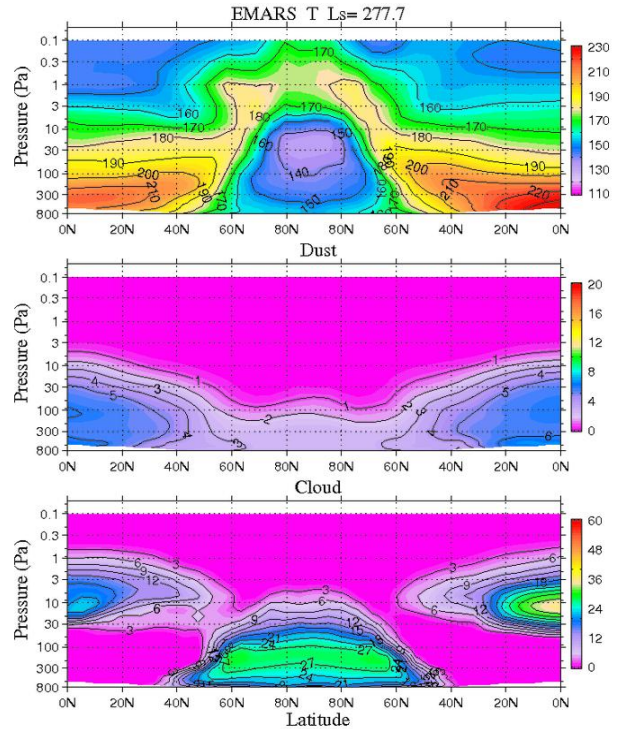


Figure 6: EMARS northern hemisphere zonal cross-sections of temperature structure (top), and the mass mixing ratios of dust (center) and water ice (bottom) for northern winter ($L_s=277.7^{\circ}$) obtained from reanalysis of MCS data (Figure 4).